

Original article

Pore-scale numerical simulation of spontaneous imbibition in porous media containing fractures

Liu Yang¹, Xiaoyu Jiang¹, Mingjun Li¹*, Fei Gong¹, Guangtao Dong¹, Xiaoshan Li²

¹State Key Laboratory for Geomechanics and Deep Underground Engineering, China University of Mining and Technology (Beijing), Beijing 100083, P. R. China

²Research Institute of Exploration and Development, PetroChina Xinjiang Oilfield Company, Karamay 834000, P. R. China

Keywords:

Phase field
two-phase flow
fractured porous media
spontaneous imbibition

Cited as:

Yang, L., Jiang, X., Li, M., Gong, F., Dong, G., Li, X. Pore-scale numerical simulation of spontaneous imbibition in porous media containing fractures. *Capillarity*, 2024, 10(2): 48-56. <https://doi.org/10.46690/capi.2024.02.03>

Abstract:

Spontaneous imbibition is an essential mechanism for recovering oil from low-permeability fractured water-driven reservoirs. To accurately capture the migration interface of oil-water two-phase flow under these conditions, this study employs phase field theory coupled with Cahn-Hilliard and Navier-Stokes equations. We conduct a numerical pore-scale investigation on countercurrent imbibition in low-permeability fractured porous media. The results show that pore-scale spontaneous imbibition can be divided into four stages. In the first stage, oil-water film is formed when oil contacts with water, and this contact line moves under the action of capillary force. In the second stage, the oil film at the end of the oil cluster ruptures to form isolated oil droplets. In the third stage, these oil droplets are surrounded by water and gradually transported outward. In the final stage, oil droplets accumulate in the fractures and are collectively expelled from the matrix. In the process of oil droplet migration, the phenomenon of sticking occurs under the influence of water extrusion and the internal structure of the matrix, which leads to the formation of residual oil. The increased complexity of open boundary and fracture development strengthens the imbibition effect by elevating the degree of spontaneous imbibition pore utilization, thus improving the oil utilization efficiency. The above findings can provide a numerical modeling reference for the study of spontaneous imbibition in fractured porous media, and at the same time, has some guiding significance for the development of low-permeability reservoirs.

1. Introduction

With the increasing energy demand in recent years, improving reservoir recovery has become the main focus of oil and gas exploitation. Fractured reservoirs, such as shale and tight sandstone, constitute a significant portion of remaining oil reserves; they are widely distributed around the world and have the characteristics of low permeability, low porosity and thus present several production challenges. Large-scale volumetric fracturing can realize the economic exploitation of low-permeability reservoirs (Wu et al., 2013). Driven by capillary

force, the water-based fracturing fluid in the hydraulic fracture system is spontaneously imbibed into the matrix system and displaces the oil in the matrix pores. This process is considered as key to increased recovery (Behbahani et al., 2006; Yang et al., 2023). Therefore, it is important to study the mechanism of spontaneous imbibition in porous media to improve oil recovery (Kazemi et al., 1976; Guo et al., 1998).

The basic hydrostatic and kinetic problems of spontaneous imbibition in porous media are among the current international hot research topics. The Lucas-Washburn (LW) imbibition model for wetting fluids was developed by combining the

kinetic factors for analyzing the spontaneous imbibition of water in single capillaries and porous media (Lucas, 1918; Washburn, 1921). Handy (1960) assumed that the spontaneous imbibition of water is a piston displacement process and established the water imbibition model of gas-saturated core on the premise of ignoring the gas phase pressure gradient of the water phase front. However, the fuzzy physical meaning of some parameters in the formula made the application of this model difficult. It was subsequently modified by combining the experimental measurements while considering the influence of initial water saturation, and the linear relationship between the spontaneous imbibition efficiency of effluent and reciprocal gas recovery efficiency was derived (Li and Horne, 2000). Amico and Lekakou (2002) studied the axial spontaneous imbibition of a single fiber bundle based on Darcy's law and established the equation of imbibition time as a function of imbibition height. Zahasky and Benson (2019) systematically analyzed the modified and extended form of LW equation for the spontaneous imbibition of porous media and studied the spontaneous imbibition rule of saturated media considering factors such as original water saturation and matrix size based on fractal theory. Cai et al. (2011) comprehensively discussed the research status of reservoir imbibition and imbibition coefficient. Based on the fractal characteristics of reservoir rock pore structure, they established a fractal model of imbibition coefficient of porous media in low-permeability reservoirs. At the same time, the prediction of the imbibition mass and coefficient fractal model was carried out, which showed good agreement with the experimental results, constituting the deepening of the fractal study of porous media spontaneous imbibition.

When imbibition occurs, the difference in contact mode and location distribution of two phase fluids may lead to completely divergent imbibition rules and seepage characteristics. Also, variation in the contact mode and positional distribution of the two phases during spontaneous imbibition may lead to highly different imbibition mechanisms and imbibition characteristics. At the same time, the instability of the two-phase fluid interface and the complicated pore filling mechanism in the imbibition process also make it difficult to predict the imbibition law. Therefore, numerical simulation has become an important tool for studying the law of spontaneous imbibition in porous media (Dong and Chatzis, 1995; Meng et al., 2019). Recently, the simulation of two-phase flow has become increasingly diversified, with the commonly used simulation methods mainly including the level-set method (Prodanovic and Bryant, 2006), the Lattice Boltzmann method (Ahrenholz et al., 2008), and the phase-field method (Cornelissen et al., 2007). The Lattice Boltzmann method is suitable for systems with complex boundary conditions, but when simulating high-density and high-viscosity fluids, the numerical simulation results are more volatile and less accurate (Hatiboglu and Babadagli, 2008; Meakin and Tartakovsky, 2009). By comparing the two simulation methods in terms of accuracy, running time and ability to capture different physical phenomena during two-phase displacement at the pore scale, Amiri et al. (2013) pointed out that the phase field method is a reliable computational method for

capturing the pore scale fluid flow mechanism in complex porous media. By coupling the phase field interface equations and Navier-Stokes equations, Rokhforouz and Akhlaghi (2017) discussed the imbibition law in single-fracture porous media and confirmed that the phase field model can realistically respond to the pore-scale spontaneous imbibition phenomena.

To date, some scholars have carried out abundant and productive research in the field of spontaneous imbibition in porous media, yet the detailed pore-scale mechanism of the imbibition process has not yet been fully clarified. Because of the complexity of low-permeability porous media, it is challenging to use core experiments and mathematical models to directly respond to the actual stratigraphic conditions. In this work, based on the phase field method coupling the Cahn-Hilliard equation and the Navier-Stoke equation, and then using the finite element method for calculation, the spontaneous imbibition mechanism is studied at pore scale. This approach allows for accurately capturing the physical phenomena of the oil-water two-phase migration interface and describing the microscopic imbibition flow mechanism in detail. The results can clarify the physical phenomena of the oil-water two-phase migration interface and describe the microscopic imbibition flow mechanism in detail.

2. Numerical model

2.1 Model geometry and boundary conditions

A finite element model of dual-media spontaneous imbibition was established using the coupled multiphysics field software COMSOL Multiphysics, and pore-scale simulations were performed using the phase-field method. The geometric size of the model was 15 mm × 10 mm, and five kinds of circular particles with different radii were randomly generated in this rectangular region using MATLAB. The rectangular fractures were 15 mm in length and 1 mm in width. The matrix was initially filled with saturated oil, the density and kinetic viscosity of which were respectively set to 840 kg/m³ and 0.02 Pa·s.

The density and kinetic viscosity of the injected water were respectively set to 1,000 kg/m³ and 0.02 Pa·s. The two-phase contact angle was set to $\pi/6$ (i.e., fixed wettability condition) and the surface tension was set to 25 N/m. The fracture inlet-exit boundary was set as shown in Fig. 1(a). The inlet was set as a fixed flow rate boundary condition, and the outlet was set as a constant pressure boundary condition (standard atmospheric pressure). The left, right and upper boundaries of the pore medium were set symmetrically. The pore walls were considered to have no-slip boundary conditions.

The geometric model and mesh sectioning are shown in Figs. 1(a) and 1(b), respectively. The more stable backward difference formulation implicit algorithm was used for the computational solutions, which computation type is transient and the solution time step and termination time were respectively set to 0.0001 and 1 s. The calculation domain was divided by free triangular mesh and encrypted by conventional methods. The more narrow the pore throat, the finer the grid. The number of overall cells after dividing the grid was 41,800, the number of boundary cells was 7,708, the number of vertex

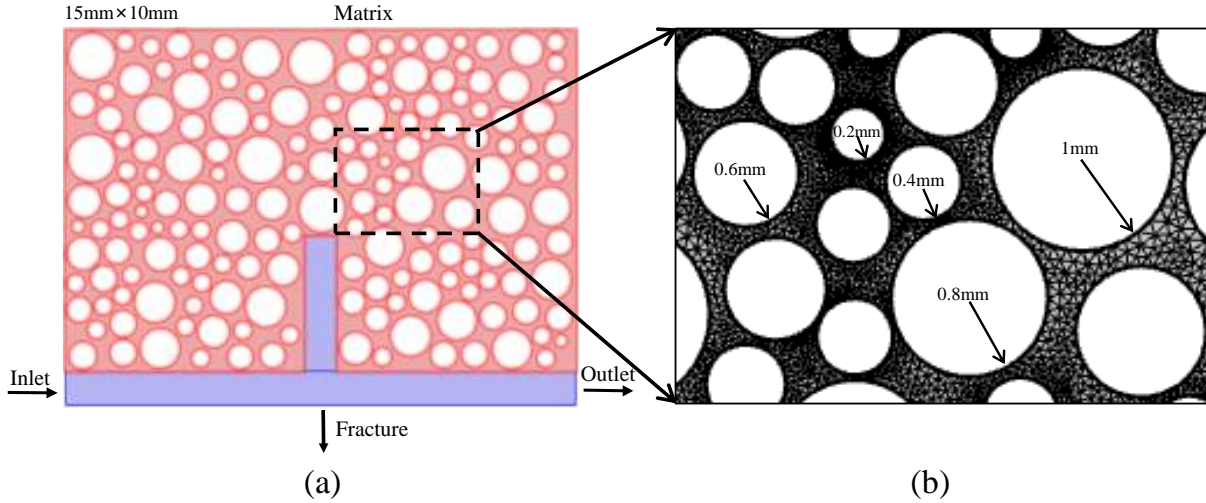


Fig. 1. Geometric model and mesh sectioning. (a) Simplified Dual Medium Geometry Model and (b) mesh discretization.

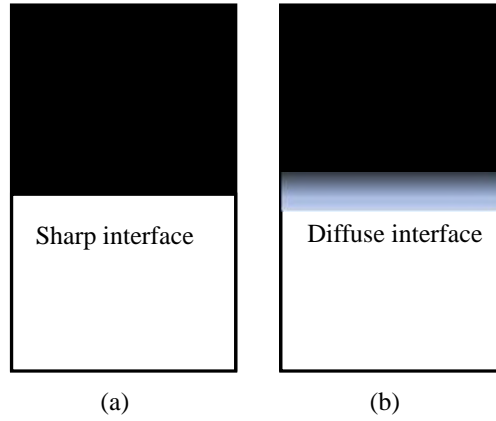


Fig. 2. Schematic of interface diffusion between two phases. (a) Traditional interface and (b) phase field interface.

cells was 704, and the average grid quality was 0.8029.

2.2 Governing equations and numerical scheme

When fluid flows in porous media, there is an obvious phase interface between different fluid phases, and the imbibition process mainly occurs in the exchange process between oil and water phases. Therefore, research on the spontaneous imbibition process primary focuses on the precise location and capture of oil-water interface. According to the phase field theory, in a small area of the phase interface, there is a diffused interface layer of a certain thickness in the interface fluid (Fig. 2(b)), but this is not in a sharp state (Fig. 2(a)).

In this paper, the phase field method was used to study the spontaneous imbibition patterns in microscopic porous media, which represents the two-phase interface as an isosurface of the phase-field function. It is capable of handling complex topological algorithms while using an approximate model, and also of accurately capturing the fluid interface during microscopic two-phase displacements (Liu et al., 2023). The oil-water two-phase moving interface was tracked by the

coupling of the Navier-Stokes and Cahn-Hilliard equations.

The phase field method uses continuously and rapidly changing phase field variables (Eq. (1)) to represent the regional position of each phase fluid and the dynamic change of the two-phase interface, in which the interface position can be quickly and accurately tracked. Here, ϕ is the phase field variable, which varies continuously from -1 to 1. Where x represents the position vector, t represents the time. Fluid 1 represents the oil phase, fluid 2 represents the water phase, and the interval between -1 and 1 represents the oil-water interface, as shown in Fig. 3:

$$\phi = \begin{cases} \phi(x,t) = -1 & \text{Fluid 1} \\ \phi(x,t) \in (0,1) & \text{Fluid interface} \\ \phi(x,t) = 1 & \text{Fluid 2} \end{cases} \quad (1)$$

Fluid flow in PF simulation consists of two parts: that in the fracture system and that in the matrix system (Jafari et al., 2017). At the same time, the oil-water two-phase fluid in the two parts of the system will also interact with each other

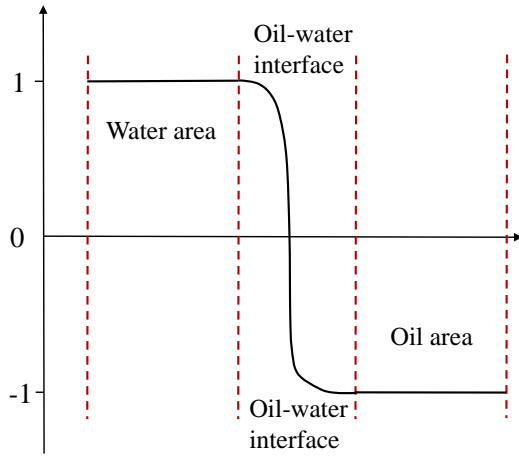


Fig. 3. Schematic diagram of the oil-water phases of the phase field variable.

when flowing. For the two-phase flow simulated by PF, the following assumptions are made: the fluid flow is laminar and is described using the Navier-Stokes equations; fluids in porous media are assumed to be Newtonian fluids and incompressible; miscibility does not occur between two phases of fluid; the viscous pressure drop is negligible. On this basis, the equation for controlling two-phase flow in dual-medium systems can be obtained.

(1) Equation of Motion

$$\rho \frac{\partial u}{\partial t} + \rho (u \nabla) u = \nabla [-PI + \kappa] + F \quad (2)$$

$$F = \left(\frac{\lambda}{\varepsilon_{pf}^2} \psi - \frac{\partial f}{\partial \phi} \right) \nabla \phi \quad (3)$$

where u denotes the fluid velocity field, ρ represents the fluid density, P represents pressure, F represents the volumetric force on the fluid, κ represents the mean curvature of the interface, ψ is an auxiliary variable of the phase field, ε_{pf} represents the thickness of the control interface for the phase field parameter, I represents the unit tensor, f is a user-defined free energy and ϕ is the capillary width corresponding to the thickness of the dispersive interface between the two phases. Eq. (2), i.e., the Navier-Stokes equation (momentum conservation equation), describes the momentum conservation during the flow of a viscous incompressible fluid.

(2) Continuity equation

$$\nabla u = 0 \quad (4)$$

The practical significance of the continuity equation is that the velocity dispersion is 0, which controls the conservation of mass during fluid flow while the volume remains constant.

(3) Two-phase flow interface control equation

$$\lambda = \frac{3\varepsilon_{pf}\sigma}{\sqrt{8}}, \gamma = \chi\varepsilon_{pf}^2, \psi = \text{PSI} \quad (5)$$

$$\frac{\partial \phi}{\partial t} + u \nabla \phi = \nabla \left(\frac{\gamma\lambda}{\varepsilon_{pf}^2} \nabla \psi, \phi = \text{PHIP}f \right) \quad (6)$$

$$\psi = \nabla \varepsilon_{pf}^2 \nabla \phi + (\phi^2 - 1)\phi + \frac{\varepsilon_{pf}^2}{\lambda} \frac{\partial f}{\partial \phi} \quad (7)$$

Eqs. (5)-(7) are the phase field interface control equations, where γ represents surface energy density, λ represents mixing energy density, σ represents two-phase interfacial tension and the two-phase fluid interfacial tension is equal to the integral of the free energy density at the interface, i.e., $\sigma = 2\sqrt{2}\lambda$, and χ is the phase field mobility tuning parameter:

$$V_{f1} = \frac{1 - \phi}{2} \quad (8)$$

$$V_{f2} = \frac{1 + \phi}{2} \quad (9)$$

$$V_{f1} + V_{f2} = 1 \quad (10)$$

$$\rho = \rho_1 V_{f1} + \rho_2 V_{f2} \quad (11)$$

$$\mu = \mu_1 V_{f1} + \mu_2 V_{f2} \quad (12)$$

where V_{f1} and V_{f2} represent the two-phase fluid volume fractions, ρ_1 and ρ_2 represent the two-phase fluid density magnitudes, μ represent the dynamic viscosity and μ_1 and μ_2 are the two-phase fluid viscosity magnitudes, respectively.

(4) Boundary condition control equations

$$n \frac{\gamma\lambda}{\varepsilon_{pf}^2} \nabla \psi = 0 \quad (13)$$

$$n \varepsilon_{pf}^2 \nabla \phi = \varepsilon_{pf}^2 \cos \theta_w |\nabla \phi| \quad (14)$$

where n represents the normal unit vector, θ_w represents the contact angle.

3. Results and discussion

3.1 Analysis of pore-scale imbibition mechanism

The oil-water distribution at different times of the One-End-Open boundary conditions is presented in Fig. 2. In this work, the One-End-Open model was used to discuss the law of spontaneous imbibition flow in dual media systems. The red liquid is the oil phase, and the blue liquid is the water phase. The dynamic simulation results of oil-water imbibition are illustrated in Fig. 2. The matrix was initially saturated with oil phase, then imbibition occurred in the system after constant-rate water injection, and finally the oil gradually discharged along the fracture.

After the continuous injection of water into the fracture from left to right at a constant rate, the matrix undergoes spontaneous imbibition driven by capillary forces, displacing the oil from the pores into the fracture and ultimately discharging it from the matrix in the form of oil droplets. Combined with the capillary force formula $P_c = 2\sigma \cos \theta / R$, the capillary force is inversely proportional to the pore throat radius, where θ represents the contact angle R represents the equivalent radius of the oil drop droplet. The capillary force is small and the viscous force plays a leading role in the position where the pore throat is larger. The heterogeneity of pore throat leads to the uneven distribution of capillary

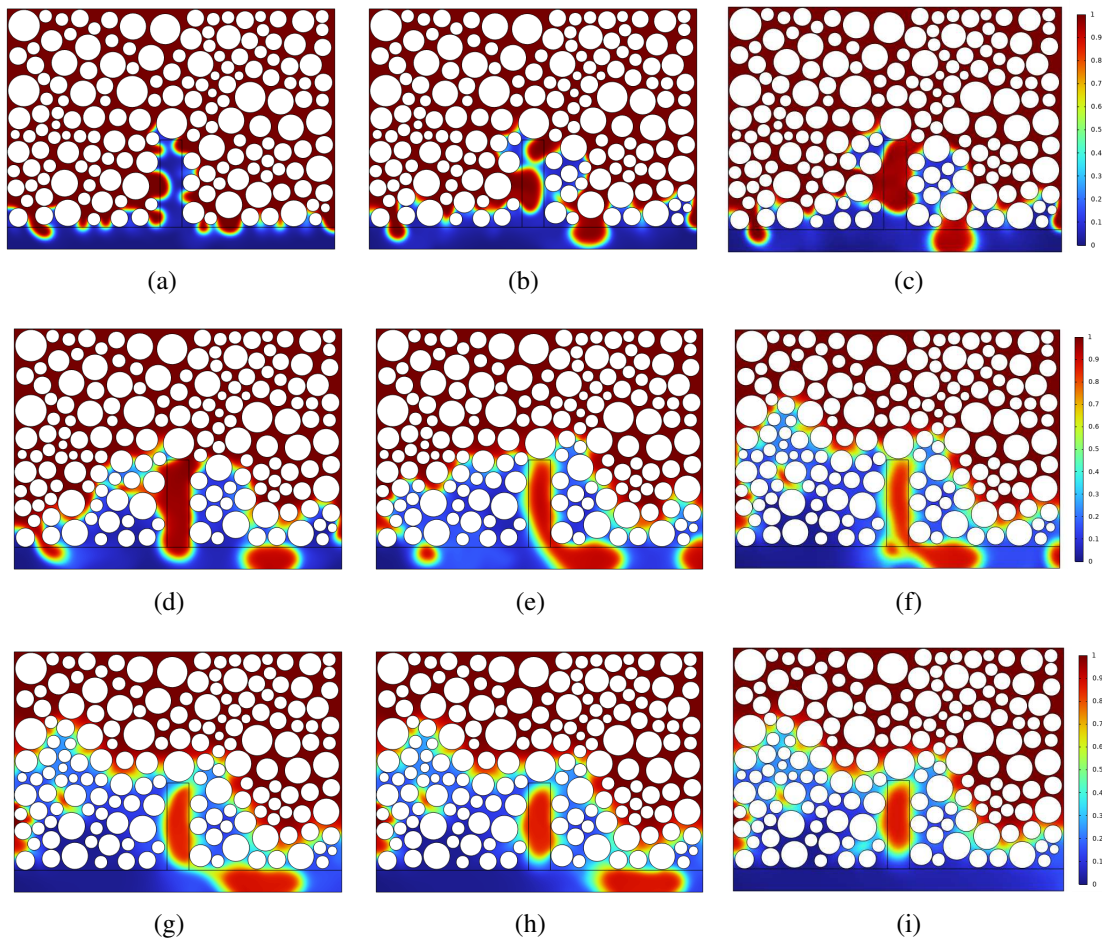


Fig. 4. Oil-water distribution at different moments of imbibition. (a) 0.01 s, (b) 0.02 s, (c) 0.05 s, (d) 0.08 s, (e) 0.1 s, (f) 0.3 s, (g) 0.4 s, (h) 0.5 s and (i) 1 s.

forces in the matrix, so the oil front does not spread uniformly but migrates from the larger pore throat to the fracture in the form of a convex liquid surface. After imbibition has occurred, water is preferentially drawn into the matrix along the small pore throats (high capillary force) and then gradually enters the dispersed pore throat connected with the pore throat, while the oil is driven from the matrix to the fracture along the larger pore throat.

As shown in Figs. 4(b)-4(d), with the passage of time, some oil droplets in the cluster contact and converge with each other, and then form large columnar oil cluster. During this period, the end of the cylindrical oil cluster does not break and continues to gather in the fracture, while the end of the drip oil film breaks and forms isolated oil droplets moving slowly outward along the fracture. At $t = 0.1$ s, the oil film at the end of the cylindrical oil cluster is completely broken under the action of water extrusion, and the oil cluster is completely released into the fracture, forming an *L*-shaped oil cluster that continues moving. At this time, water in the fractures under spontaneous imbibition has carried more isolated oil droplets. As shown in Fig. 4(f), different sizes of oil droplets of in the fracture have different transportation speeds. Under the influence of velocity difference, some isolated oil droplets

converge with each other and further fuse to form large oil clusters that move continuously. At this time, a number of oil droplets have been discharged from the matrix.

At the matrix-fracture junction, the oil phase as a non-wetting phase is squeezed by the water in the fracture. Eventually, the *L*-shaped oil clusters are stuck, and part of the matrix is discharged along the fracture under the action of continuous water flow. The imbibition equilibrium state is shown in Fig. 4(i). In the position far away from the fracture, if water cannot be further displaced into the matrix far away from the fracture, then the oil phase loses the drive of the capillary suction force, and finally becomes bound in the pores to form the imbibition remaining oil.

The enlarged cross-sections of different locations in the matrix for the imbibition process are shown in Fig. 5. Multiphysics simulation software successfully captures the microscopic phenomena, such as thinning and rupture of the oil film, movement of the fluid contact line, water bridging, and oil droplet detachment. When oil and water come into contact, the interface will first form an oil-water film and then start the oil-water contact line movement under the action of capillary force. As shown in Fig. 5(a), the pore throats between particles 4 and 5 on both sides of the fracture are significantly larger

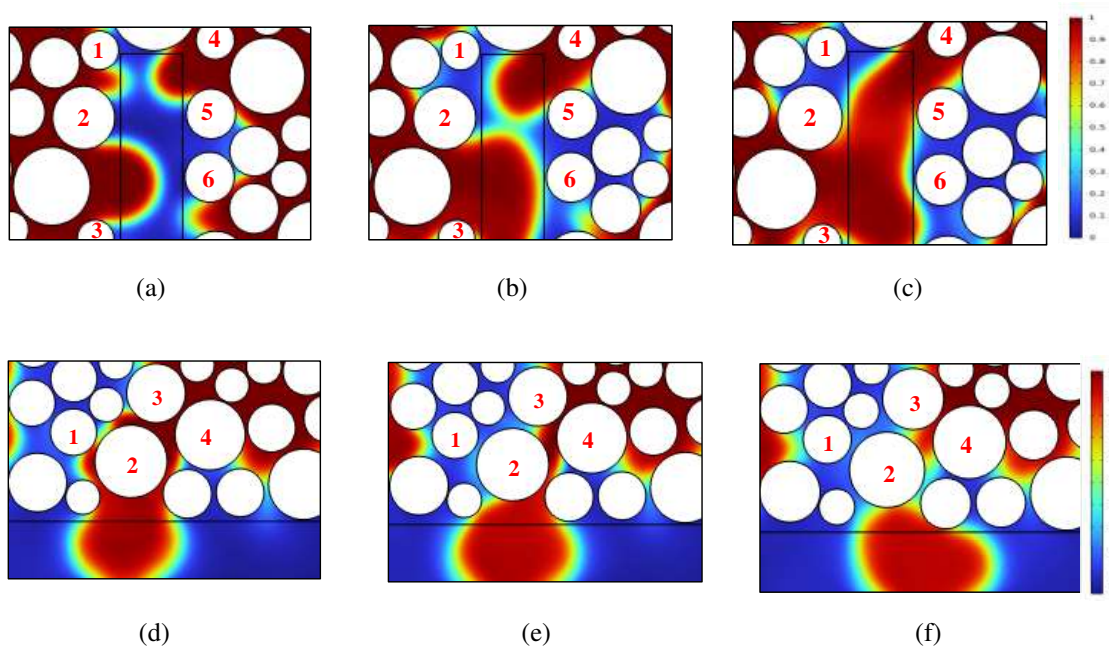


Fig. 5. Enlarged screenshot of different imbibition times at different positions of the model during imbibition process. (a) Converged interface: $t = 0.01$ s, (b) converged interface: $t = 0.05$ s, (c) converged interface: $t = 0.1$ s, (d) snap off interface: $t = 0.01$ s, (e) snap off interface: $t = 0.05$ s and (f) snap off interface: $t = 0.1$ s.

than those between particles 5 and 6. The capillary force is relatively small, so the dominant viscosity force is strong. It is the main channel for spontaneous imbibition, and the displacement of matrix oil is relatively large. In the process of oil droplet movement, after the front curved surfaces of multiple oil droplets have come into contact, they aggregate to form larger oil clusters and then continue to move outward along the fracture.

When the oil cluster moves along the fracture, a water bridge is formed in the throat of adjacent matrix particles, resulting in the gradual thinning of the oil film. Finally, under the action of water compression, the end of the oil cluster breaks, forming completely isolated oil droplets that are released into the fracture. The pore throat between particles 1 and 2 in Fig. 5(b) is significantly smaller than that between particles 2 and 3. Water is preferentially drawn into the small pore throat with higher capillary force (i.e., between particles 1 and 2), and the oil film in this pore throat is the first to break under the pressure of water. Then, the oil film in the larger pore throat between particles 2 and 3 is broken and isolated oil droplets are formed, which are finally discharged under continuous water flow.

The distribution of pressure field and velocity field at different self-priming moments is shown in Fig. 6. The pressures within the oil and water phase regions in the matrix are different, and there is a capillary pressure difference between the oil and water layers as a driving force for spontaneous imbibition. When $t = 0.01$ s after imbibition occurs, the pressure at the convex liquid surface of the oil phase front is lower than that in the internal oil domain, and the capillary driving force is larger, which means that continuous imbibition

will occur at these locations. At this time, the oil phase has a higher flow rate, and combined with the velocity field distribution diagram, it can be seen that the capillary driving force and velocity are greater at the position with a smaller pore throat, consistent with the formula of capillary force.

When the end of the oil mass has completely split to form an isolated oil droplet, the internal and external pressure difference decreases with the increase in the size of the formed droplet, and the oil droplet increases the resistance of water flow through the fracture. Combined with the pressure field distribution diagram for $t = 0.1$ s, it can be seen that the smaller the isolated oil droplet, the greater the surface pressure of the oil film and the larger the pressure difference that will be formed. This is consistent with $\Delta p = 2\sigma R$, where Δp represents the pressure difference between the inside and outside of the droplet. As shown by the velocity field cloud image in Fig. 6(b), oil droplets in fractures gradually increase with spontaneous imbibition, and fluid velocity gradually slows down. After the end of imbibition, all the movable oil droplets are discharged. At this time, water flows slowly in the fracture, and the fluid velocity and pressure of the joint surface tend to be stable.

3.2 Influence of fracture development area on imbibition

The final distribution of oil and water after double media imbibition under different fracture development conditions is shown in Fig. 7. It can be seen that the increase in fracture development has obvious influence on imbibition. As shown in the simulation results, the larger the fracture extension area and complexity of the joint surface, the greater the imbibition

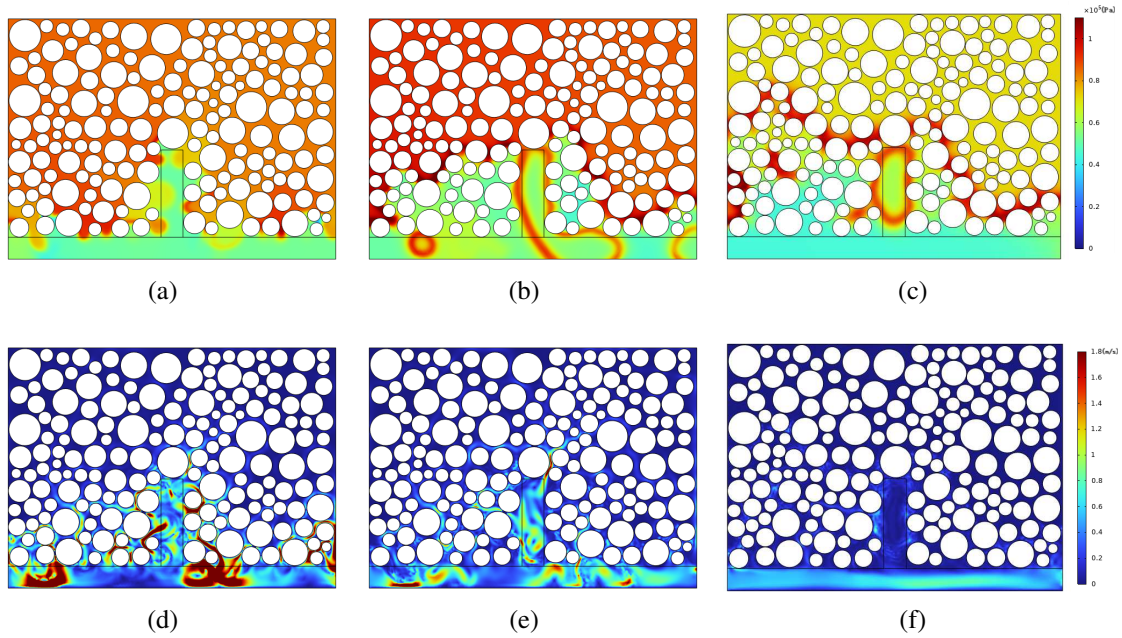


Fig. 6. Pressure and velocity fields at different moments of imbibition. (a) Pressure field: $t = 0.01$ s, (b) pressure field: $t = 0.1$ s, (c) pressure field: $t = 1$ s, (d) velocity field: $t = 0.01$ s, (e) velocity field: $t = 0.1$ s and (f) velocity field: $t = 1$ s.

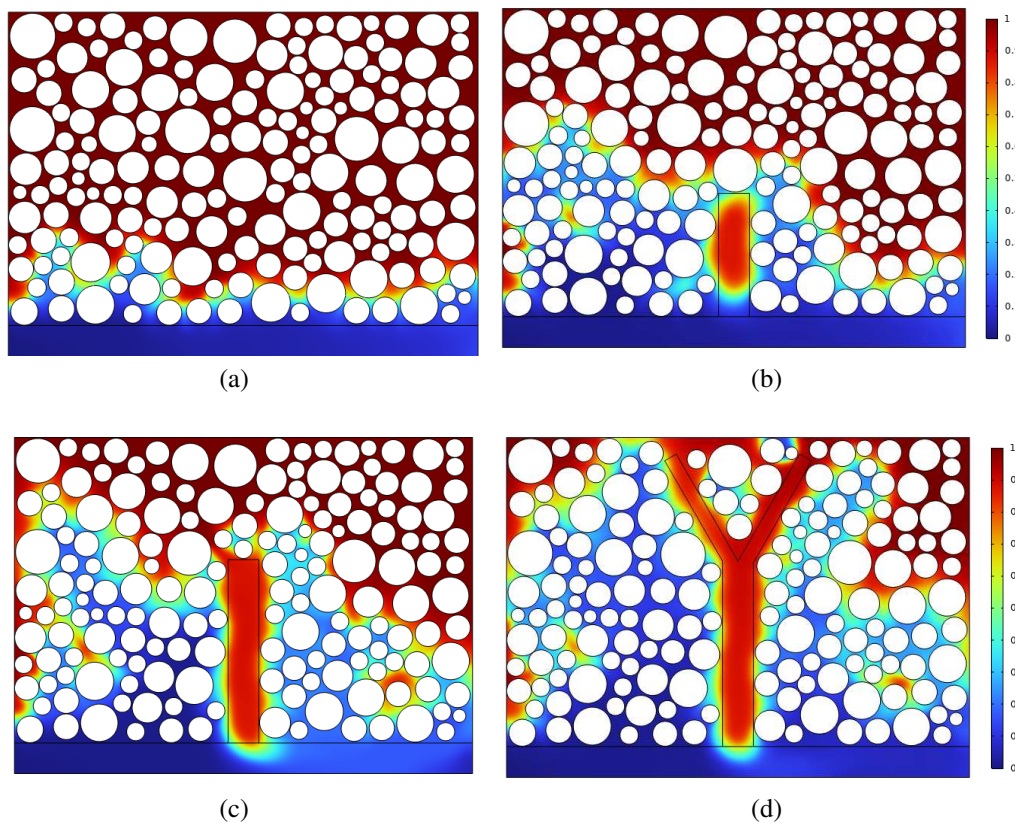


Fig. 7. Final distribution of oil and water at the end of double medium imbibition. (a) No fractures in the matrix, (b) 4 mm vertical fracture, (c) 6 mm vertical fracture and (d) Y-shaped fracture.

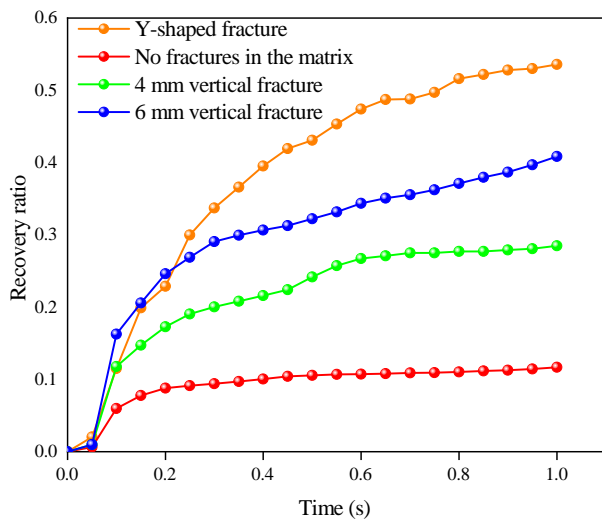


Fig. 8. Variation curves of fracture recovery for different complexities.

sweep range and the lower the final residual oil volume.

When bifurcated fractures develop in the matrix, the imbibition efficiency is the highest, as shown in Fig. 7(d), and the residual oil in the matrix pores is significantly lower than the other three media. One reason for this phenomenon is that oil is displaced by water into fractures, where it can be collected and discharged more easily. In addition, the presence of bifurcated fractures also allows water to be drawn deeper into the matrix while enabling more pores to participate in the imbibition process. The efficiency of crude oil recovery during spontaneous imbibition is subsequently improved.

The development of fractures has a significant impact on the ultimate recovery rate of spontaneous imbibition, as shown in Fig. 8. The higher the fracture development degree, the wider the imbibition sweep and the higher the ultimate oil recovery. Although the trend of recovery curve is upward, the slope of recovery curve and final recovery rate vary among cases.

The slopes of the four curves at the beginning of imbibition are similar and almost coincide, and this part corresponds to the process where oil droplets begin to be displaced by water into the fracture. The mean capillary radius of the matrix without fractures is small, and the pore participation rate is low during imbibition. The recovery curves are first flattened at about 0.5 s, the recovery rate is low, and the maximum recovery rate is 11.67%. With the increasing fracture area in the matrix, more pores are exposed and the average capillary radius increases, so the imbibition effect is gradually enhanced. The strongest imbibition effect is found in the case of *Y*-shaped fractures developed in the matrix. Before 0.2 s, the fracture development area and the average capillary radius along the matrix joint of *Y*-type fracture are the largest, and the most oil is discharged into the fracture during the imbibition process. In the process of oil drops moving away from the matrix, the resistance causes slow oil drops moving in the early stage, so the recovery curve of 6 mm vertical fracture before 0.2 s is slightly higher than that of *Y* fracture. Subsequently, the oil drop is discharged outward with the water flow, and the

recovery rate increases gradually. The oil droplets are then discharged outward with the water flow and the recovery rate is gradually improved. The maximum slope of *Y* fracture matrix recovery curve means that the imbibition rate is faster, and the final recovery rate is as high as 53.59%.

4. Conclusions

In this paper, a two-phase flow model was established based on the phase field method, and the pore scale spontaneous imbibition process was described in detail. Moreover, the influence of different fracture development on the recovery rate was studied. The main conclusions are drawn as follows:

- 1) The overall imbibition process can be divided into four stages: the first stage is the formation of oil film after oil-water contact and the advancement of oil-water contact line movement; the second stage is the formation of isolated oil droplets; the third stage is the outward transportation of oil droplets surrounded by water; the fourth stage is the pooling and discharging of oil droplets in the fractures.
- 2) The phenomenon of sticking occurs during the transport of spontaneous imbibition oil droplets. The internal structure of porous media is complex and the oil droplets are prone to snapping off when squeezed by water at the fracture-matrix junction. The oil cluster is split into two parts; one part is exported to the matrix along the fracture, while the other part is lost to the capillary force drive and will remain in the matrix to form residual oil. This phenomenon will affect the ultimate oil recovery of spontaneous imbibition.
- 3) After the beginning of imbibition, the pressure at the convex liquid surface of the oil phase front becomes lower than that in the internal oil domain, and the capillary driving force is larger, which is the premise of continuous imbibition. At the same time, the smaller the isolated oil droplets formed in the process of imbibition, the higher the surface pressure of the oil film and the higher the difference between surface and internal pressure.
- 4) The imbibition effect is gradually strengthened with the progression of fracture development. The increase in joint fracture length and the extension of secondary bifurcation fracture will enlarge the exposed area of matrix pores, and water can penetrate deeper into the matrix to make the spontaneous imbibition spread to a wider area. This is conducive to improving the efficiency of crude oil utilization and enhancing imbibition recovery.

Acknowledgements

This work was supported by the Natural Science Foundation of China (No. 52374014), the National Key R&D Program of China (No. SQ2022YFE020645), and the Fundamental Research Funds for the Central Universities (No. 2022YQSB03).

Conflict of interest

The authors declare no competing interest.

Open Access This article is distributed under the terms and conditions of

the Creative Commons Attribution (CC BY-NC-ND) license, which permits unrestricted use, distribution, and reproduction in any medium, provided the original work is properly cited.

References

- Ahrenholz, B., Tolke, J., Lehmann, P., et al. Prediction of capillary hysteresis in a porous material using lattice-Boltzmann methods and comparison to experimental data and a morphological pore network model. *Advances in Water Resources*, 2008, 31(9): 1151-1173.
- Amico, S. C., Lekakou, C. Axial impregnation of a fiber bundle. Part 1: Capillary experiments. *Polymer Composites*, 2002, 23(2): 249-263.
- Amiri, H. A. A., Hamouda, A. A. Evaluation of level set and phase field methods in modeling two phase flow with viscosity contrast through dual-permeability porous medium. *International Journal of Multiphase Flow*, 2013, 52: 22-34.
- Behbahani, H. S., Donato, G. D., Blunt, M. J., Simulation of counter-current imbibition in water-wet fractured reservoirs. *Journal of Petroleum Science and Engineering*, 2006, 50(1): 21-39.
- Cai, J., Zhao, C., Tan, L., et al. Fractal analysis of imbibition coefficient of porous media in low permeability reservoir. *Geological Science and Technology Information*, 2011, 30(5): 54-59.
- Cornelissen, J. T., Taghipour, F., Escudié, R., et al. CFD modelling of a liquid-solid fluidized bed. *Chemical Engineering Science*, 2007, 62(22): 6334-6348.
- Dong, M., Chatzis, I. The imbibition and flow of a wetting liquid along the corners of a square capillary tube. *Journal of Colloid and Interface Science*, 1995, 172(2): 278-288.
- Guo, B., Schechter, D. S., Baker, R. O. An integrated study of imbibition waterflooding in the naturally fractured Spraberry. Paper SPE 39801 Presented at SPE Permian Basin Oil and Gas Recovery Conference, Midland, Texas, 23-26 March, 1998.
- Handy, L. L. Determination of effective capillary pressures for porous media from imbibition data. *Transactions of the AIME*, 1960, 219(1): 75-80.
- Hatiboglu, C. U., Babadagli, T. Pore-scale studies of spontaneous imbibition into oil-saturated porous media. *Physical Review E*, 2008, 77(6): 066311.
- Jafari, I., Masihi, M., Nasiri, M. Numerical simulation of counter-current spontaneous imbibition in water-wet fractured porous media: Influences of water injection velocity, fracture aperture, and grains geometry. *Physics of Fluids*, 2017, 29(11): 113305.
- Kazemi, H., Jr, L. S. M., Porterfield, K. L., et al. Numerical simulation of water-oil flow in naturally fractured reservoirs. *Society of Petroleum Engineers Journal*, 1976, 16(6): 317-326.
- Li, K., Horne, R. N. Characterization of spontaneous water imbibition into gas-saturated rocks. Paper SPE 62552 Presented at the SPE/AAPG Western Regional Meeting, Long Beach, California, 19-23 June, 2000.
- Liu, Q., Li, J., Liang, B., et al. Complex wettability behavior triggering mechanism on imbibition: A model construction and comparative study based on analysis at multiple scales. *Energy*, 2023, 275: 127434.
- Lucas, R. Rate of capillary ascension of liquids. *Kolloid-Zeitschrift*, 1918, 23(15): 15-22.
- Meakin, P., Tartakovsky, A. M. Modeling and simulation of pore-scale multiphase fluid flow and reactive transport in fractured and porous media. *Reviews of Geophysics*, 2009, 47(3): RG3002.
- Meng, Q., Cai, J., Wang, J. Scaling of countercurrent imbibition in 2D matrix blocks with different boundary conditions. *SPE Journal*, 2019, 24(3): 1179-1191.
- Prodanovic, M., Bryant, S. L. A level set method for determining critical curvatures for drainage and imbibition. *Journal of Colloid and Interface Science*, 2006, 304(2): 442-458.
- Rokhforouz, M. R., Akhlaghi, A. H. A. Phase-field simulation of counter-current spontaneous imbibition in a fractured heterogeneous porous medium. *Physics of Fluids*, 2017, 29(6): 062104.
- Washburn, E. W. Dynamics of capillary flow. *Physical Review Journals Archive*, 1921, 17(3): 273-283.
- Wu, Y., Li, J., Zhang, X., et al. Numerical simulation of low-permeability fractured reservoirs on imbibition. *Advanced Materials Research*, 2013, 712: 792-795.
- Yang, L., Wang, H., Xu, H., et al. Experimental study on characteristics of water imbibition and ion diffusion in shale reservoirs. *Geoenergy Science and Engineering*, 2023, 229: 212167.
- Zahasky, C., Benson, S. M. Spatial and temporal quantification of spontaneous imbibition. *Geophysical Research Letters*, 2019, 46(21): 11972-11982.